

Support Information

for

Component-specific biochar from biomass fractions regulates radical/non-radical pathway selectivity for organics degradation

Shujing Ye ^{a, b*}, Qi Zhao ^{a, b}, Junda Chen ^{a, b}, Jiadi Hu ^{a, b}, Shangpan Yang ^{a, b}, Yulian

Deng ^{a, b}, Caihong Li ^{a, b}, Lele Chen ^{a, b}, Ruxin Nong ^{a, b}, Xiaofei Tan^{c, d}

^a School of Resources, Environment and Materials, Guangxi University, Nanning 530004, PR China

^b Guangxi Key Laboratory of Emerging Contaminants Monitoring, Early Warning and Environmental Health Risk Assessment, Nanning 530004, PR China

^c College of Environmental Science and Engineering, Hunan University, Changsha 410082, PR China

^d Shenzhen Research Institute, Hunan University, Shenzhen 518000, PR China

Number of pages: 40

6 texts, 7 tables, 21 figures

Text S1. Preparation of biochar-based catalysts.

Text S2. Characterization of biochar-based catalysts.

Text S3. Experimental procedure of boehm titration

Text S4. Measure method of PDS.

Text S5. The method of the amendatory contribution calculation.

Text S6. Electrochemical test.

Table S1. Oxygen content and configuration of biochar-based by XPS (at.).

Table S2. Content of oxygen-containing groups on biochar surface determined by Boehm titration method

Table S3. Structure analysis of HBC, HRBC, and HLBC based on Raman deconvolution.

Table S4. The value of k_{obs} ($\times 10^{-3}$, min^{-1}) in immediate degradation.

Table S5. The degradation rate among different biochar catalysts

Table S6. The value of k_{obs} ($\times 10^{-3}$, min^{-1}) in delayed addition degradation.

Table S7. The value of k_{obs} ($\times 10^{-3}$, min^{-1}) in MeOH quenching trial.

Fig S1. FT-IR absorption spectra of Walnut, residue, and lignin.

Fig S2. FT-IR absorption spectra of HBC, HRBC, and HLBC.

Fig S3. The high resolution XPS spectrum of C 1s of HBC(a), HRBC(b), and HLBC(c).

Fig. S4. Electron spin resonance analysis of HLBC.

Fig S5. SEM images of proto-lignin (a), HLBC (b), HBC (c and d), HRBC (e and f), HRTEM image of HLBC (g), HBC (h) and HRBC (i).

Fig. S6. The anti-interference test of HBC, HRBC, and HLBC.

Fig. S7. The cycle degradation test of HBC, HRBC, and HLBC.

Fig. S8. The efficiency contribution distribution of HBC and HRBC (calculated based on quenching trial).

Fig. S9. Electron spin resonance analysis of HBC, HRBC, and HLBC by using DMPO

as trapping agents in biochar/PDS system.

Fig. S10. The PDS decomposition in Biochar/PDS/TCH system with and without the presence of L-histidine.

Fig. S11. Electron spin resonance analysis of HBC, HRBC, and HLBC by using TEMP as trapping agents in biochar/PDS system.

Fig. S12. OHBC (Pre-oxidized HBC), OHRBC, and OHLBC on the oxidation and removal ratio of TCH by PDS.

Fig. S13. The correlation between PDS consumption and k_{obs} of HBC in controlled and delayed oxidation process.

Fig. S14. The correlation between PDS consumption and k_{obs} of HRBC in controlled and delayed oxidation process.

Fig. S15. The correlation between PDS consumption and k_{obs} of HLBC in controlled and delayed oxidation process.

Fig. S16. The efficiency contribution distribution of HBC, HRBC, and HLBC.

Fig. S17. Trends in hydroxyl content and radical contribution values among HBC, HRBC and HLBC.

Fig. S18. Trends in the ratio of A_G/A_Σ and ETP contribution values among HBC, HRBC and HLBC.

Fig. S19. Open circuit potential of HBC (a), and HRBC (b) electrode after adding PDS and TCH.

Fig. S20. Cyclic voltammetry curves of TCH on graphite electrode during pH 5-9.

Fig. S21. Electrochemical impedance spectroscopy (EIS) results of HBC, HRBC, and HLBC.

Text S1. Preparation of biochar-based catalysts.

The lignin extraction procedure was refined based on the previous research findings. Specifically, the preparation of deep eutectic solvents (DES) involved mixture of ChCl and Urea at a molar rate of 1:2 in a round-bottomed flask, conducted by magnetic stirring and heating at 85°C until a clear, viscous liquid was obtained without noticeable particles. Walnut shell powder (60 mesh) was then mechanically stirred with the prepared DES (the mass ratio of walnut and DES is 1:5) and shifted to the polytetrafluoroethylene (PTFE) liner of a high-pressure reactor, which was maintained at 155°C for 9 h. After cooling to room temperature, the mixture was gradually transferred to a volume of ethanol (99.7%) under continuous stirring. Following mixing thoroughly for 6 hours, the insoluble component called residue was separated by filtration and subsequently dried at 60 °C. The filtrate was then subjected to rotary evaporation to recycle the ethanol. The none-evaporable component was transferred back to PTFE liner and proceeded with thermal carbonation at 190 °C for 12 h. Upon cooling to room temperature, the solution collected in the PTFE liner following by adding excess deionized water to precipitate the lignin. Once complete precipitation was achieved, the lignin was filtered from the aqueous solution and washed multiple times with deionized water to ensure the effective removal of ethanol. Finally, after a drying at room temperature, the proto-lignin was obtained. The walnut shell powders, residue, and proto-lignin were collected for further characterization and preparation.

For the synthesis of biochar, the above dried precursors were ground and sieved to 60 mesh before being transferred to tubular furnace for pyrolysis reaction. Given that the conventional pyrolysis procedures under limited oxygen condition can cause the agglomeration and melting of lignin, a novel and improved protocol of pyrolysis was designed: (1) walnut, residue, proto-lignin were heated to 250°C at a rate of 5°C/min and then held for 30 min; (2) the temperature was increase to 450°C at a rate of 1°C/min and maintained for 60 min; (3) finally, the temperature was raised to 800°C at 2°C/min and keep for 30 min. After cooling, the collected biochar catalysts were named HBC,

HRBC, and HLBC, respectively. These samples were repeatedly washed with deionized water to effectively wipe the ash and soluble organic compound off and stored in sealed plastic bags for further use.

Text S2. Characterization of biochar-based catalysts.

Scanning electron microscope (SEM, Hitachi Japan) was applied to characterize the morphological and structural details of biochar-based catalysts. Raman spectra, acquired from a Raman spectrometer (Renishaw inVia Reflex) assisted with 532 nm laser, was employed to determine the crystallinity of biochar-based catalysts. The element contents and chemical composition of surface were examined by X-ray photoelectron spectroscopy (XPS, Thermo scientific K-Alpha) with the calibration of C1s at 284.8 eV under Al-K α X-ray radiation. And the functional groups of the samples' surface were monitored on the basis of FTIR spectra performed in KBr pellet using Thermo IN 10 Spectrometer in a region of 4000-400 cm⁻¹. The crystallographic structure was investigated by obtaining X-ray diffraction (XRD, Bruker D8, Germany) patterns. The residual TC concentration was quantified by high performance liquid chromatograph (HPLC, Shimadzu, Japan) at detecting λ of 357 nm. HPLC performed with C-18 column (4.6 mm \times 250 mm), injection volume of 20 μ L under the temperature of 30°C. Mobile phase used for detection was acetonitrile: 0.01 M oxalic acid (1:4, v:v) with a flow rate of 1.0 mL/min.

Text S3. Experimental procedure of boehm titration

Approximately 1 g of biochar samples were weighed into four conical flasks. Each flask was then treated with 25.0 mL of standardized alkaline solutions: 0.1 M sodium ethoxide (C_2H_5ONa), 0.1 M sodium hydroxide ($NaOH$), 0.05 M sodium carbonate (Na_2CO_3), and 0.1 M sodium bicarbonate ($NaHCO_3$). The mixtures were agitated on a mechanical shaker at ambient temperature for 1 h, followed by static equilibration for 24 h. Post-filtration and thorough washing of the carbon material, the combined filtrates were treated with 50.0 mL of 0.1 M hydrochloric acid (HCl). Phenolphthalein indicator was introduced, and residual acidity was quantified via back-titration using 0.1 M $NaOH$ until a faint pink endpoint was achieved.

Text S4. Measure method of PDS.

The detection of persulfate (PDS) was employed by ultraviolet-visible (UV) spectrophotometry, where the analytical procedure necessitates the preparation of a coloring reagent comprising a concentration of 1.78 mM sodium bicarbonate and 178 mM potassium iodide. During the assay, a volume of 0.1 mL of the sample is mixed thoroughly with 4.9 mL of the coloring solution, followed by subsequent incubation in the darkness for a duration of 30 min prior to measuring the absorbance of the resultant mixture at a wavelength of 352 nm using an UV spectrophotometer. Given the potential interference of TCH degradation products, the PDS concentration was determined after five minutes of oxidation process.

Text S5. The method of the amendatory contribution calculation.

Utilize the correlation depicted in Figure 4d-f, it is possible to derive the theoretical k_{obs} obtained from MeOH quenching trial. By applying the first-order oxidation kinetics equation, one can determine the extent of quenching imparted by MeOH under identical PDS consumption conditions, thereby rectifying the contribution attributed to radical.

Pseudo first-order kinetic model:

$$\ln\left(\frac{c_t}{c_0}\right) = -k_{obs}t \quad (S1)$$

Where t is the reaction time (min), k_{obs} is the pseudo first-order rate constant, c_t and c_0 are the concentration at time t and the initial concentration of TCH, respectively.

the correlation equations of k_{obs} and PDS consumption are shown below:

$$\text{HBC:} \quad k_{obs} = (0.0406 \pm 0.003)c_{PDS} - (5.89 \pm 1.77) \times 10^{-4} \quad (S2)$$

$$\text{HBC-D10:} \quad k_{obs} = (0.0421 \pm 0.0033)c_{PDS} - (5.59 \pm 1.55) \times 10^{-4} \quad (S3)$$

$$\text{HBC-D60:} \quad k_{obs} = (0.0463 \pm 0.00921)c_{PDS} - (5.02 \pm 1.88) \times 10^{-4} \quad (S4)$$

$$\text{HRBC:} \quad k_{obs} = (0.04083 \pm 0.004)c_{PDS} - (5.35 \pm 1.60) \times 10^{-4} \quad (S5)$$

$$\text{HRBC-D10:} \quad k_{obs} = (0.0512 \pm 0.0040)c_{PDS} - (5.14 \pm 1.04) \times 10^{-4} \quad (S6)$$

$$\text{HRBC-D60:} \quad k_{obs} = (0.0539 \pm 0.00752)c_{PDS} - (5.04 \pm 1.74) \times 10^{-4} \quad (S7)$$

$$\text{HLBC:} \quad k_{obs} = (0.212 \pm 0.0428)c_{PDS} + (4.61 \pm 1.66) \times 10^{-3} \quad (S8)$$

$$\text{HLBC-D10:} \quad k_{obs} = (0.3 \pm 0.105)c_{PDS} + (2.2 \pm 3.39) \times 10^{-3} \quad (S9)$$

$$\text{HLBC-D60:} \quad k_{obs} = (1.18 \pm 0.368)c_{PDS} - (2.47 \pm 1.13) \times 10^{-2} \quad (S10)$$

Where k_{obs} is the pseudo first-order rate constant, c_{PDS} is the consumption of PDS.

The amendatory contribution of different pathway was calculated by following modified method, serving contribution of radical pathway in HBC performance as example. To mitigate the impact of reduced PDS utilization by HBC due to the addition of MeOH, the following simplified equation based on the Pseudo first-order kinetic model can be derived:

$$\frac{\ln\left(\frac{c_{t,1}}{c_{0,1}}\right)}{\ln\left(\frac{c_{t,2}}{c_{0,2}}\right)} = \frac{k_1}{k_2} \quad (\text{S11})$$

$$1 - \frac{c_{t,2}}{c_{0,2}} = 1 - e^{\frac{k_2}{k_1} \ln\left(\frac{c_{t,1}}{c_{0,1}}\right)} \quad (\text{S12})$$

Where $c_{t,1}$ and $c_{0,1}$, representing the concentration at reaction time t and initial time t_0 , can be replaced by known auxiliary point from the equation S2 for subsequent calculation; k_1 is pseudo first-order rate constant in HBC/PDS/TCH system; k_2 is a theoretical rate constant that confirms to equation S2, corresponding to the same consumption of PDS after the addition of MeOH; $c_{t,2}$ and $c_{0,2}$ represent the theoretical concentration at reaction time t and initial time t_0 , corresponding to the rate constant k_2 .

For the HBC/PDS/MeOH system at pH=3, with $\frac{c_{t,1}}{c_{0,1}}=40\%$, $c_{\text{PDS}}=4.1\%$, $k_1=3.46 \times 10^{-3} \text{ (min}^{-1}\text{)}$, substituting these values into equation S2 and S12 results in $(1 - \frac{c_{t,2}}{c_{0,2}})$ as 15% which regarded as theoretical degradation efficiency of 15% (without MeOH addition under identical PDS consumption). The actually degradation efficiency after adding MeOH is 6%, leading to an amendatory contribution of 60%.

Text S6. Electrochemical test.

(1) To determine the half-wave potential ($\phi_{1/2}$) of TCH, cyclic voltammetry (CV) was utilized with electrochemical workstation model CHI760E, employing a three-electrode system, and a platinum sheet acts as the counter electrode, a Ag/AgCl electrode functioning as the reference electrode; the electrolyte solution employed was a phosphate buffer prepared pH within 5 to 9 at a concentration of 10 mM. For CV testing, the initial and final voltage was set to -0.1 V and 1.5 V, respectively, with a scan rate set at 10 mV/s. Other conditions, such as the volume of the solution and the concentration of contaminant, remained consistent with parameters in the degradation trials.

The calculation formulas of $\phi_{1/2}$ in the reversible and irreversible system are shown in the following Eq. (S1) and (S2)

$$\phi_{1/2} = \frac{1}{2}(E_{pa} + E_{pc}) \quad (\text{S1})$$

Among the parameters, the E_{pa} represents the anodic peak potential, and E_{pc} symbolizes the cathodic peak potential.

$$\phi_{1/2} = \frac{1}{2}\left(E_p + \frac{E_p}{2}\right) \quad (\text{S2})$$

Among the parameters, E_p denotes the peak-to-peak potential, whereas the $\frac{E_p}{2}$ signifies the potential at which current is halved.

(2) To accomplish the measurement of open circuit of potential (OCP) within the system, initially, 10 mg of material was dispersed in a mixed solution of Naphthol and ethanol (volume ratio of 1:20), followed by the ultrasonic treatment for 30 min to ensure homogeneity. Subsequently, 20 μL of mixed suspended solids were slowly dripped onto a glassy carbon electrode and dried. This process was repeated three times to fabricate the working electrode. The electrodes were immersed in a 10 mM phosphate buffer until the electrochemical properties stabilized, the OCP test was conducted before and after the addition of PDS and TCH.

(3) The testing frequency was set from 0.01 Hz to 100000 Hz for electrochemical

impedance spectroscopy (EIS) measurements.

Table S1. Oxygen content and configuration of biochar-based by XPS (at.).

sample	O proportion (%)	C-O (%)	C=O (%)
HBC	9.12	3.83	5.29
HRBC	9.67	3.38	6.29
HLBC	6.03	0.00	6.03

Table S2. Content of oxygen-containing groups on biochar surface determined by Boehm titration method

	Functional groups (mmol/g)			
	Carboxyl	Lactone	Hydroxyl	Carbonyl
HBC	0.170	0.016	0.101	0.005
HRBC	0.182	0.070	0.078	0.059
HLBC	0.097	0.004	0.001	0.025

Table S3. Structure analysis of HBC, HRBC, and HLBC based on Raman deconvolution.

	Area ratio of Raman peaks (%)				
	S	D	A	G	A_D/A_A
HBC	9.50	41.8	33.40	15.30	1.25
HRBC	8.00	49.2	20.00	22.80	2.46
HLBC	6.50	53.9	14.00	25.60	3.85

Table S4. The value of k_{obs} ($\times 10^{-3}$, min^{-1}) in immediate degradation.

	pH			
	3.0	4.5	6.0	7.5
HBC	3.46	0.83	0.65	1.10
HRBC	1.94	0.64	0.61	0.83
HLBC	12.30	12.40	13.00	13.50

Table S5. The degradation rate among different biochar catalysts

Biomass	oxidant	k_{obs} (min^{-1})	Pollutant	Reference
Pig manure	PMS	0.015	Ciprofloxacin	1
Bamboo residue	PS	0.010	Tetracycline	2
Spirulina residue	PMS	0.011	Sulfamethoxazole	3
Boehmeria nivea	PDS	0.0065	Sulfamethoxazole	4
Fractionated lignin of walnut	PDS	0.014	Tetracycline	This work

Table S6. The value of k_{obs} ($\times 10^{-3}$, min^{-1}) in delayed addition degradation.

	D10				D60			
	pH							
	3.0	4.5	6.0	7.5	3.0	4.5	6.0	7.5
HBC	2.80	0.60	0.48	0.87	2.40	0.37	0.31	0.43
HRBC	1.34	0.57	0.55	0.60	1.24	0.53	0.51	0.56
HLBC	11.56	11.91	12.00	12.03	11.44	11.53	11.8	11.98

Table S7. The value of k_{obs} ($\times 10^{-3}$, min^{-1}) in MeOH quenching trial.

	pH	
	3.0	4.5
HBC	0.24	0.12
HRBC	0.27	0.19
HLBC	10.86	10.87

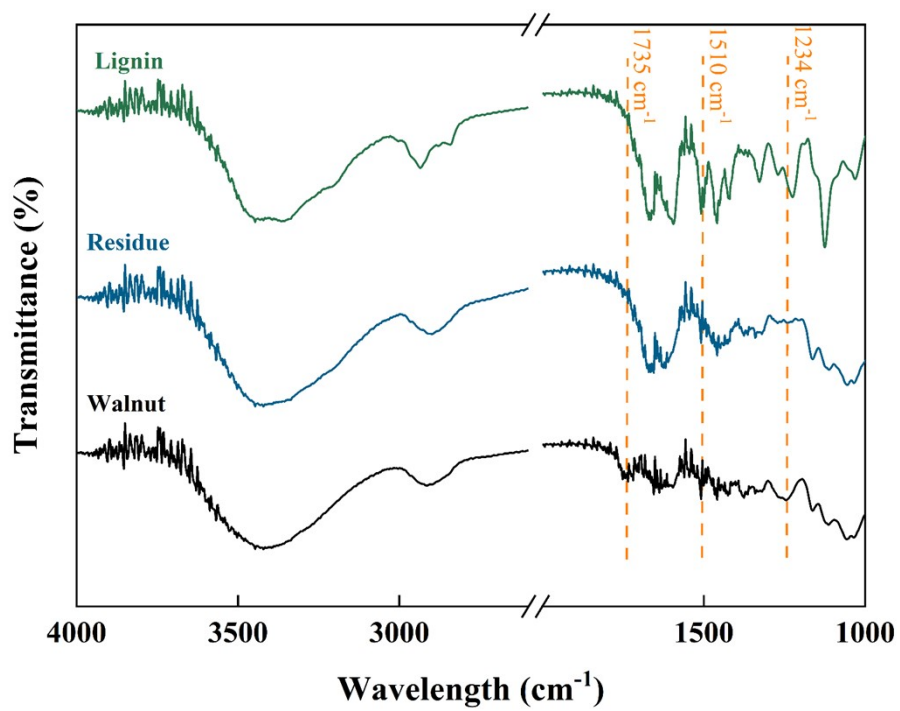


Fig. S1. FT-IR absorption spectra of Walnut, residue, and lignin.

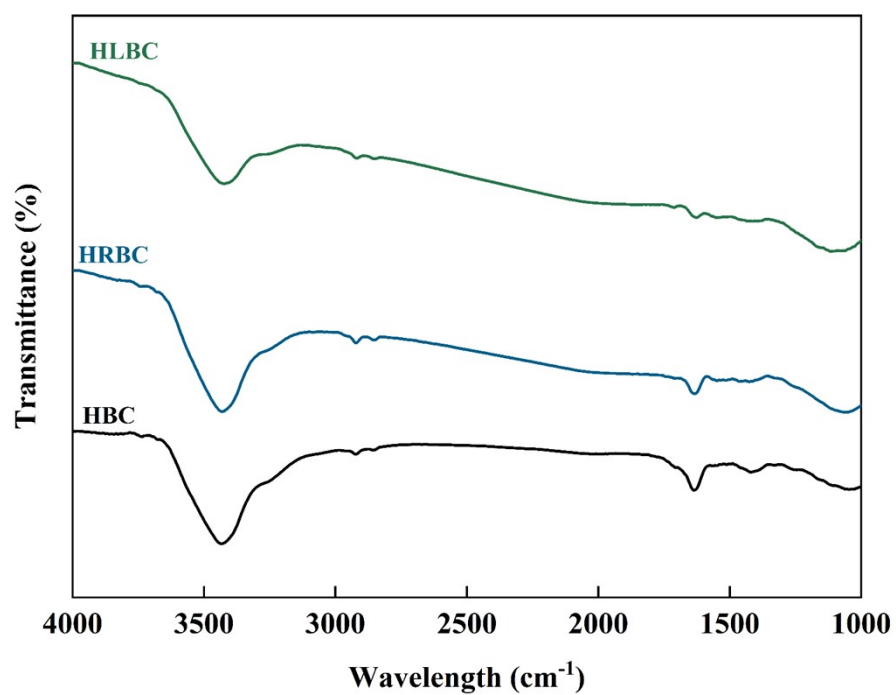


Fig. S2. FT-IR absorption spectra of HBC, HRBC, and HLBC.

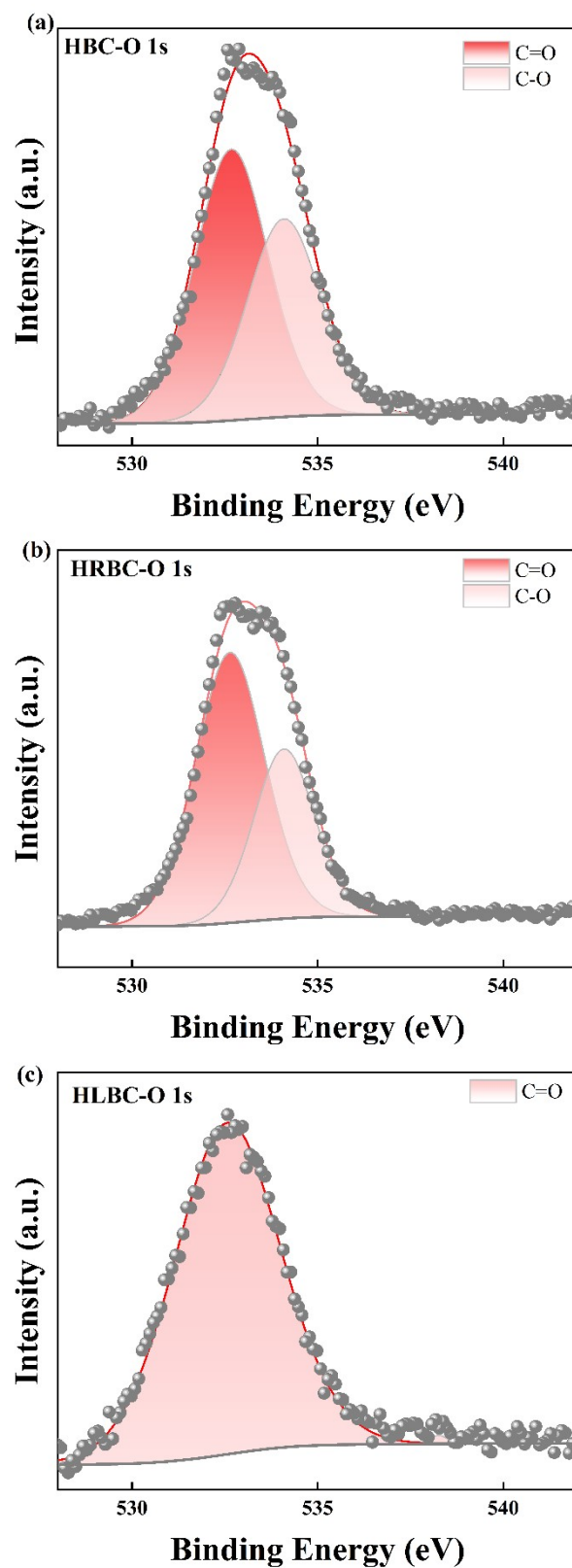


Fig. S3. The high resolution XPS spectrum of C 1s of HBC(a), HRBC(b), and HLBC(c).

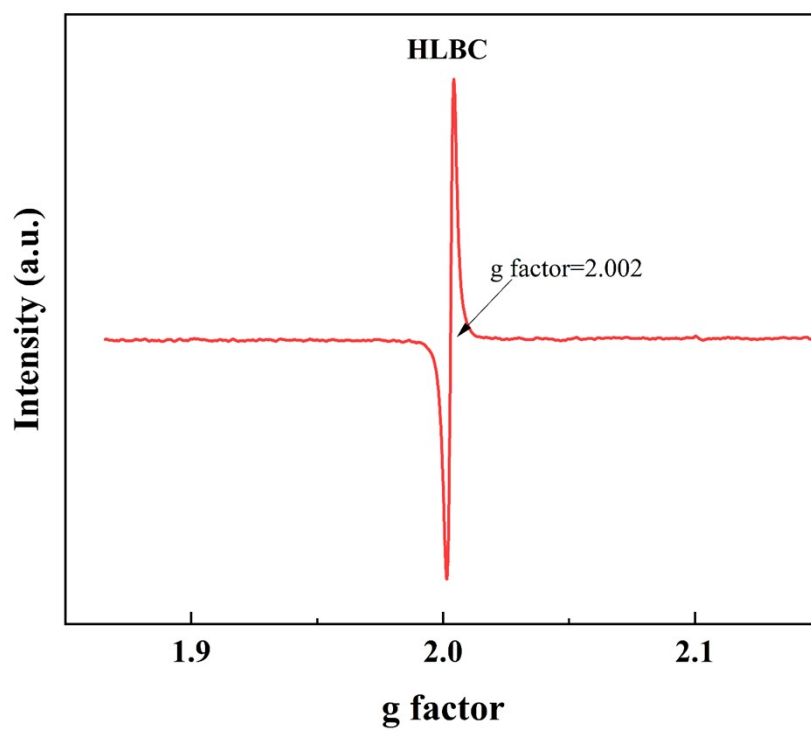


Fig. S4. Electron spin resonance analysis of HLBC.

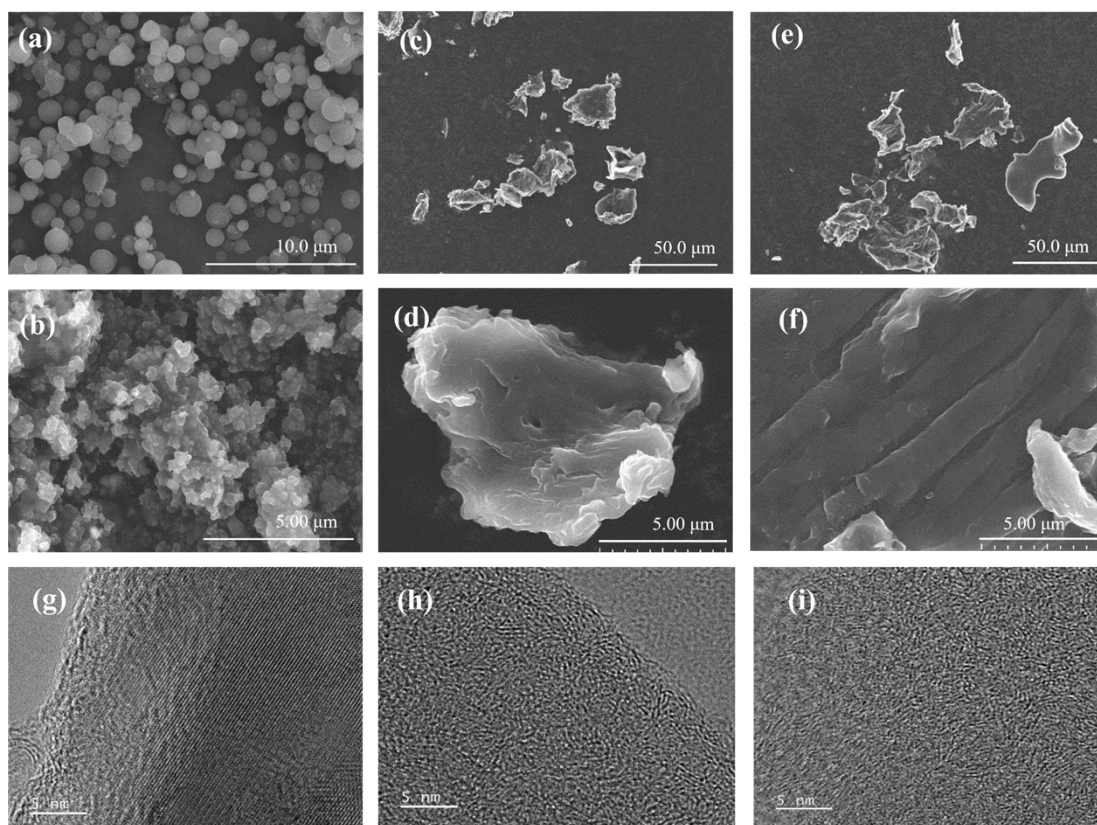


Fig. S5. SEM images of proto-lignin (a), HLBC (b), HBC (c and d), HRBC (e and f), HRTEM image of HLBC (g), HBC (h) and HRBC (i).

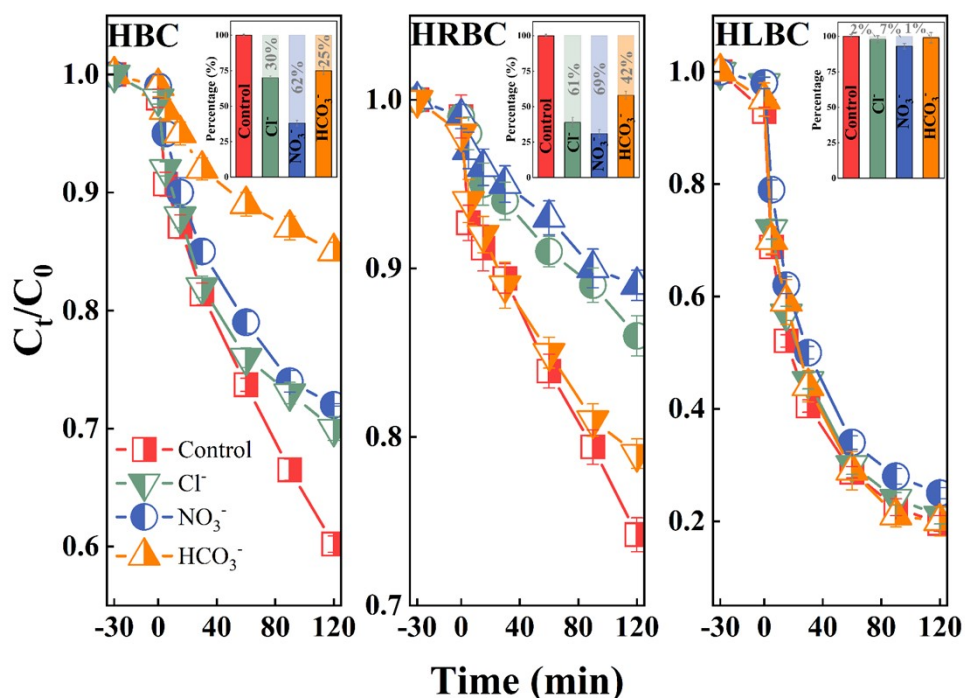


Fig. S6. The anti-interference test of HBC, HRBC, and HLBC. Condition: [biochar]=0.1 g/L, [PDS]=2 mM, [Ion concentration]=20 mM, [TCH]=10 mg/L, [temperature]=25 °C, [pH]=3.0.

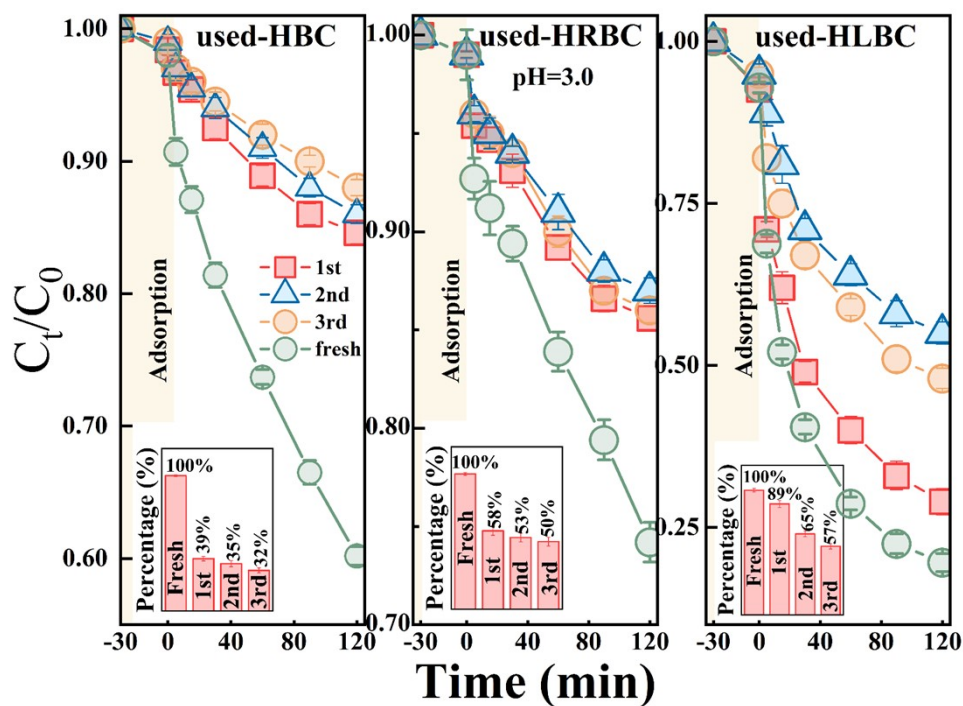


Fig. S7. The cycle degradation test of HBC, HRBC, and HLBC. Condition: [biochar]=0.1 g/L, [PDS]=2 mM, [TCH]=10 mg/L, [temperature]=25°C, [pH]=3.0.

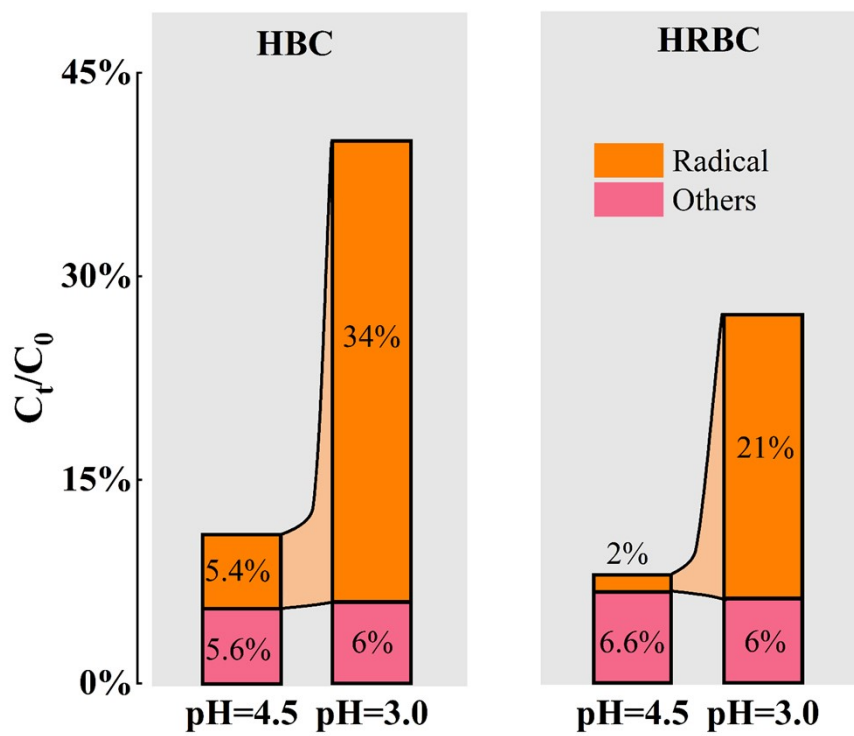


Fig. S8. The efficiency contribution distribution of HBC and HRBC (calculated based on quenching trial). Condition: [biochar]=0.1 g/L, [PDS]=2 mM, [temperature]=25°C.

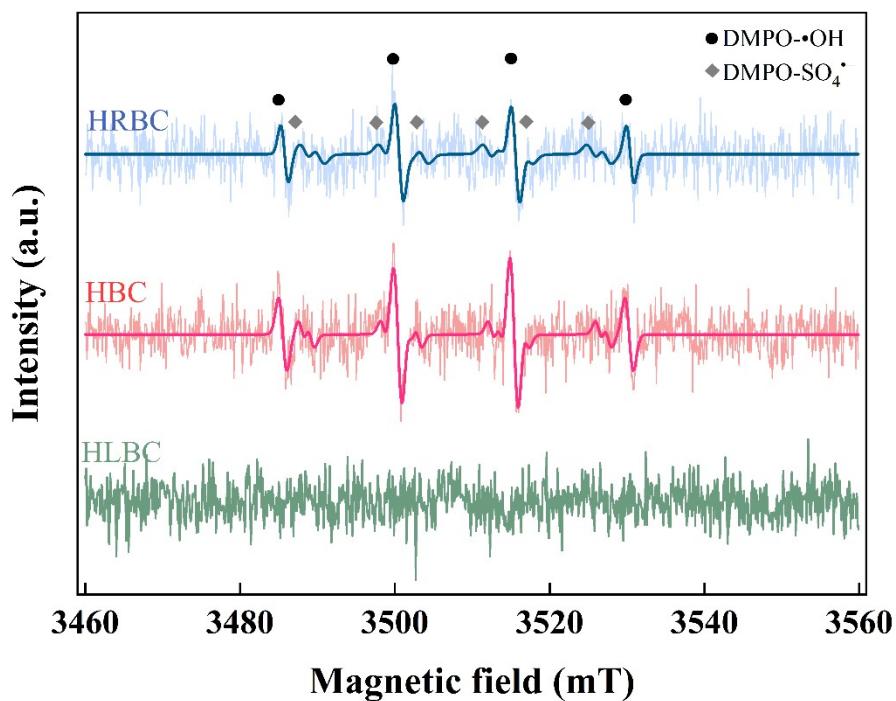


Fig. S9. Electron spin resonance analysis of HBC, HRBC, and HLBC by using DMPO as trapping agents in biochar/PDS system. Condition: [biochar]=0.1 g/L, [PDS]=2 mM, [temperature]=25°C, [pH]=3.0.

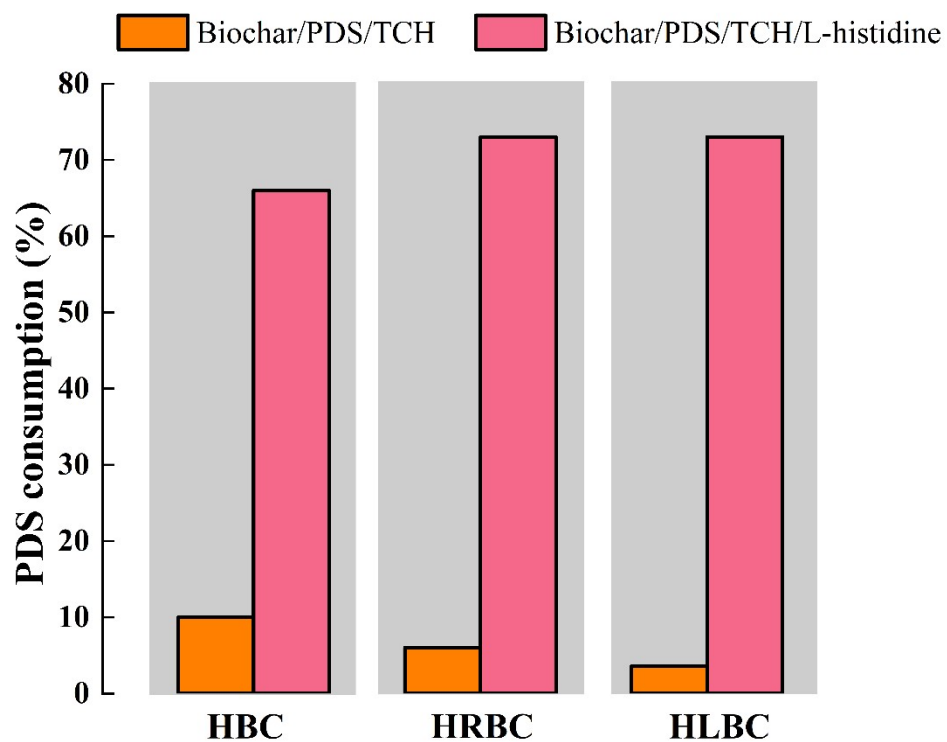


Fig. S10. The PDS decomposition in Biochar/PDS/TCH system with and without the presence of L-histidine. Condition: [biochar]=0.1 g/L, [PDS]=2 mM, [temperature]=25°C, [pH]=3.0.

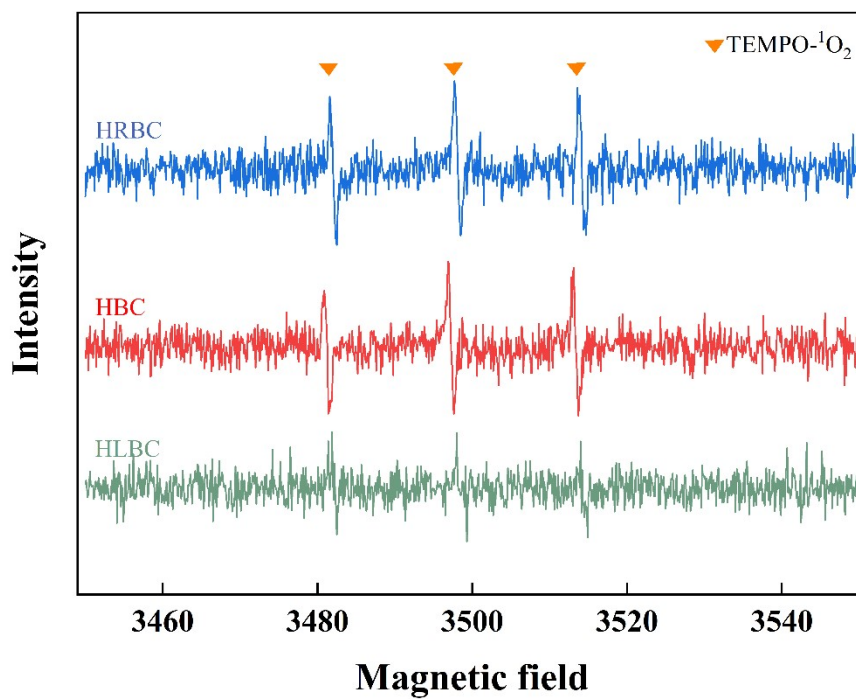


Fig. S11. Electron spin resonance analysis of HBC, HRBC, and HLBC by using TEMP as trapping agents in biochar/PDS system. Condition: [biochar]=0.1 g/L, [PDS]=2 mM, [temperature]=25°C, [pH]=3.0.

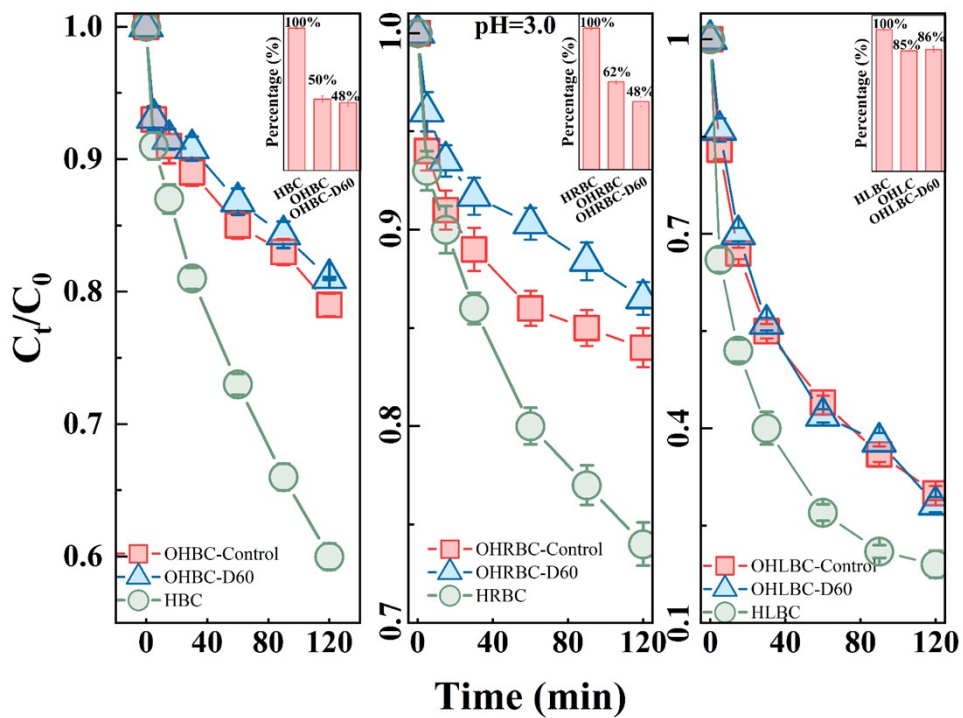


Fig. S12. OHBC (Pre-oxidized HBC), OHRBC, and OHLBC on the oxidation and removal ratio of TCH by PDS. Condition: [biochar]=0.1 g/L, [PDS]=2 mM, [temperature]=25°C, [pH]=3.0.

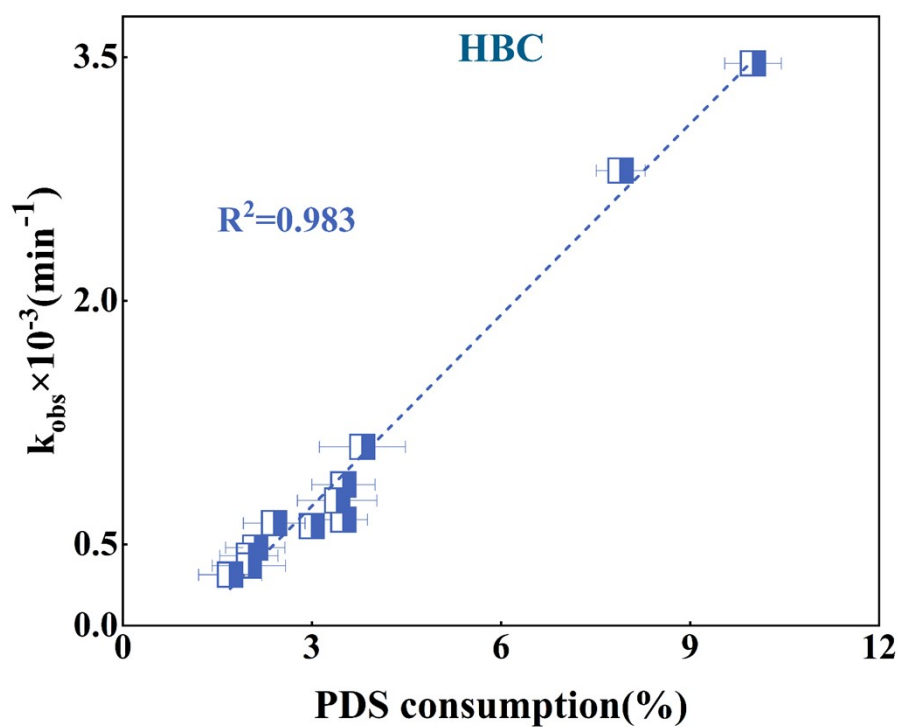


Fig. S13. The correlation between PDS consumption and k_{obs} of HBC in controlled and delayed oxidation process. Condition: [biochar]=0.1 g/L, [PDS]=2 mM, [TCH]=10 mg/L, [temperature]=25°C, [initial pH]=4.5.

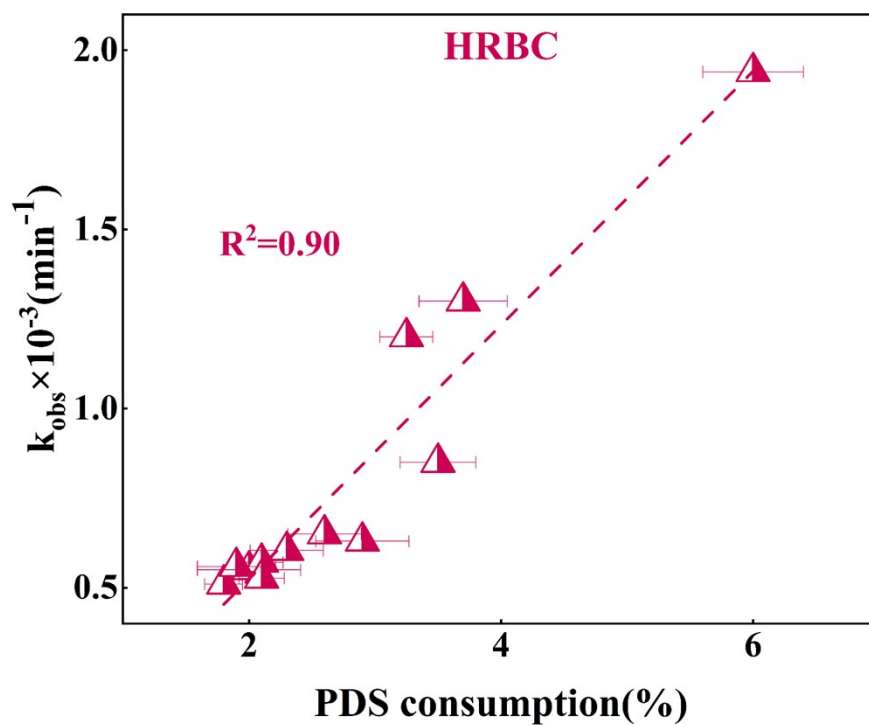


Fig. S14. The correlation between PDS consumption and k_{obs} of HRBC in controlled and delayed oxidation process. Condition: [biochar]=0.1 g/L, [PDS]=2 mM, [TCH]=10 mg/L, [temperature]=25°C, [initial pH]=4.5.

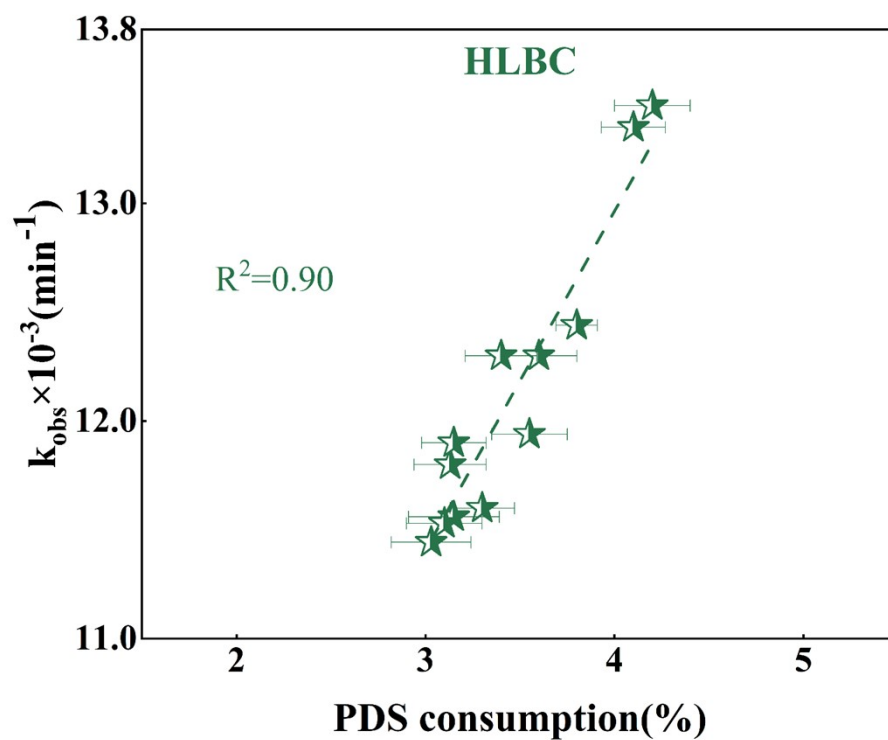


Fig. S15. The correlation between PDS consumption and k_{obs} of HLBC in controlled and delayed oxidation process. Condition: [biochar]=0.1 g/L, [PDS]=2 mM, [TCH]=10 mg/L, [temperature]=25°C, [initial pH]=4.5.

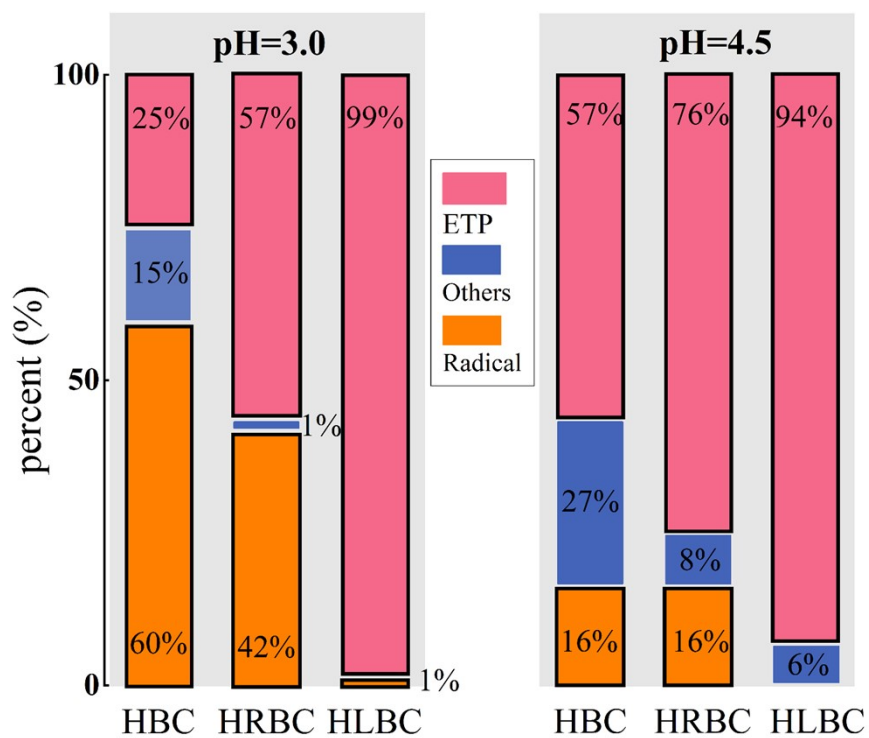


Fig. S16. The efficiency contribution distribution of HBC, HRBC, and HLBC. Condition: [biochar]=0.1 g/L, [PDS]=2 mM, [temperature]=25°C.

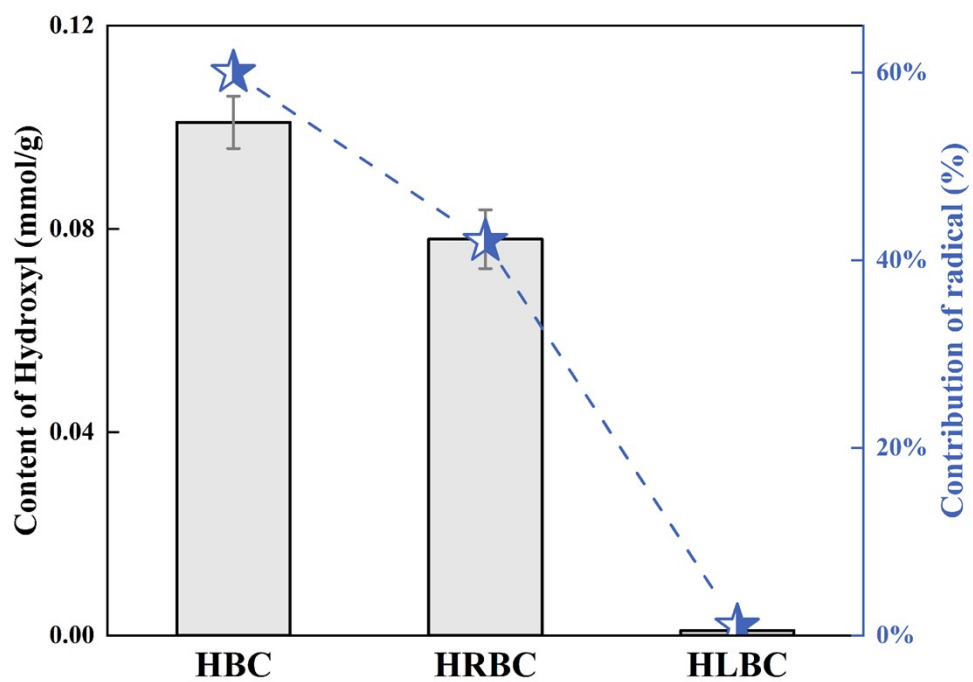


Fig. S17. Trends in hydroxyl content and radical contribution values among HBC, HRBC and HLBC.

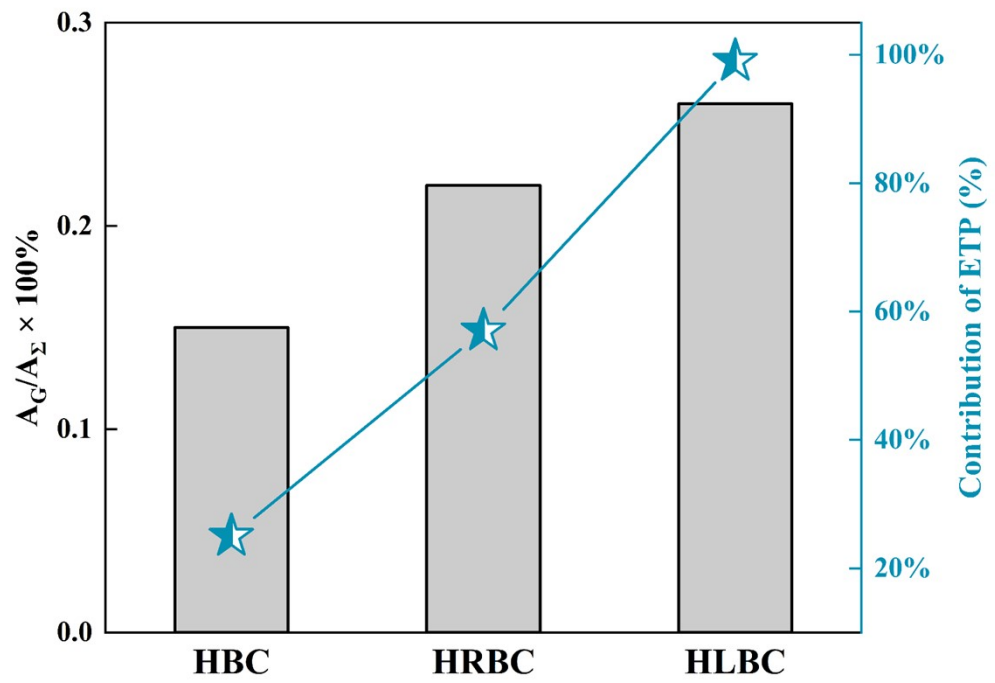


Fig. S18. Trends in the ratio of A_G/A_Σ and ETP contribution values among HBC, HRBC and HLBC.

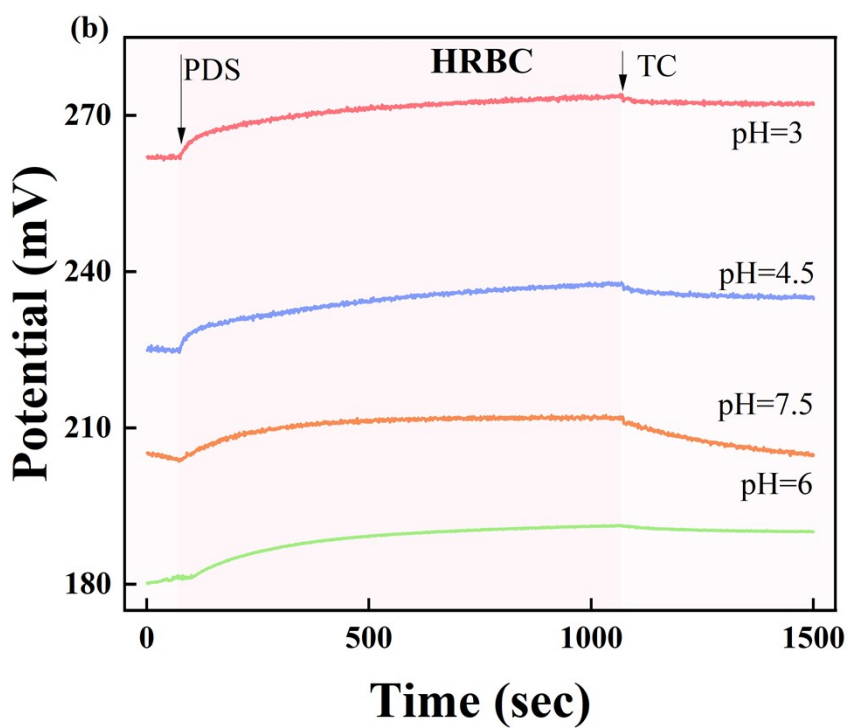
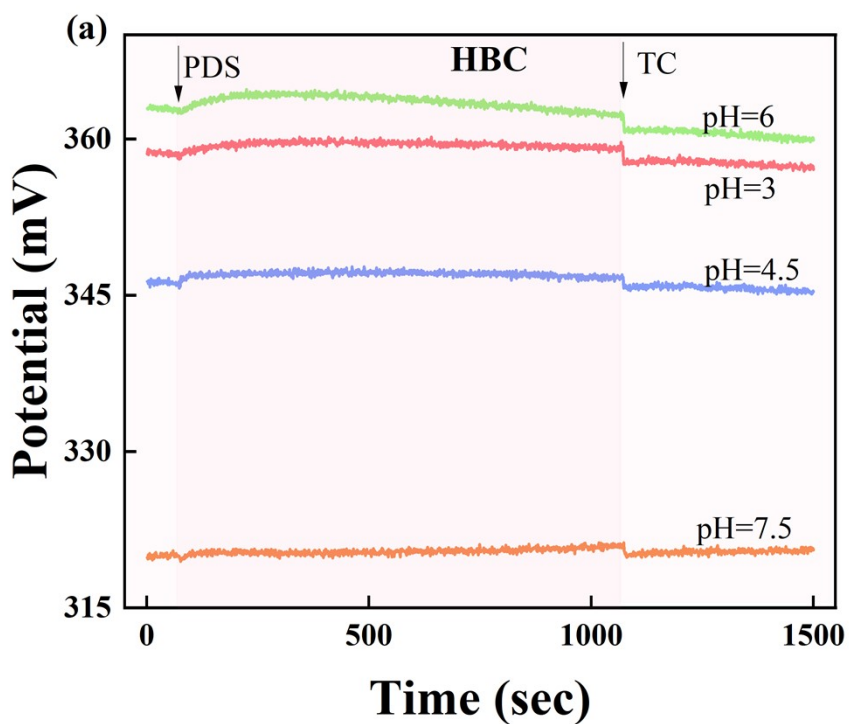


Fig. S19. Open circuit potential of HBC (a), and HRBC (b) electrode after adding PDS

and TCH.

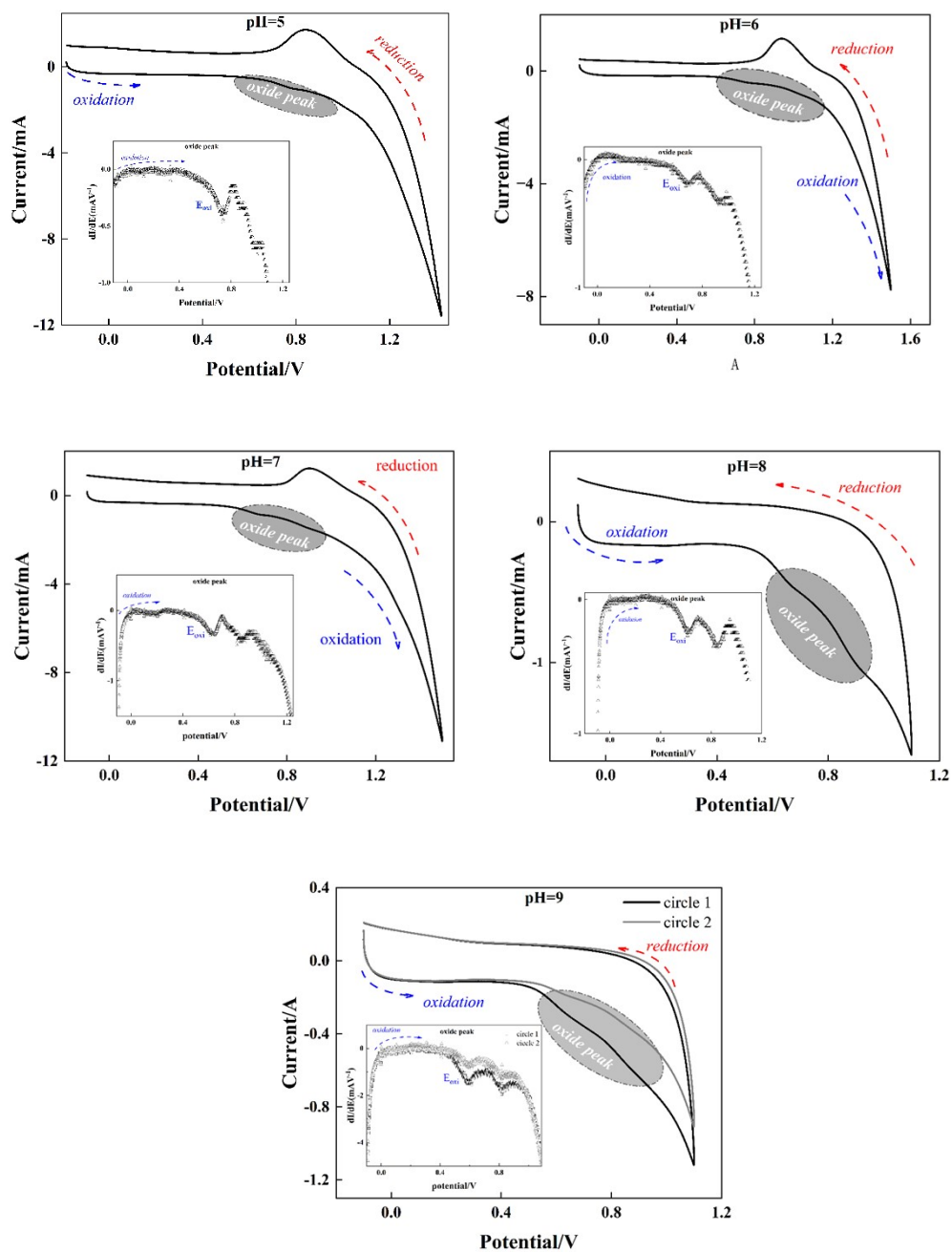


Fig. S20. Cyclic voltammety curves of TCH on graphite electrode during pH 5-9.

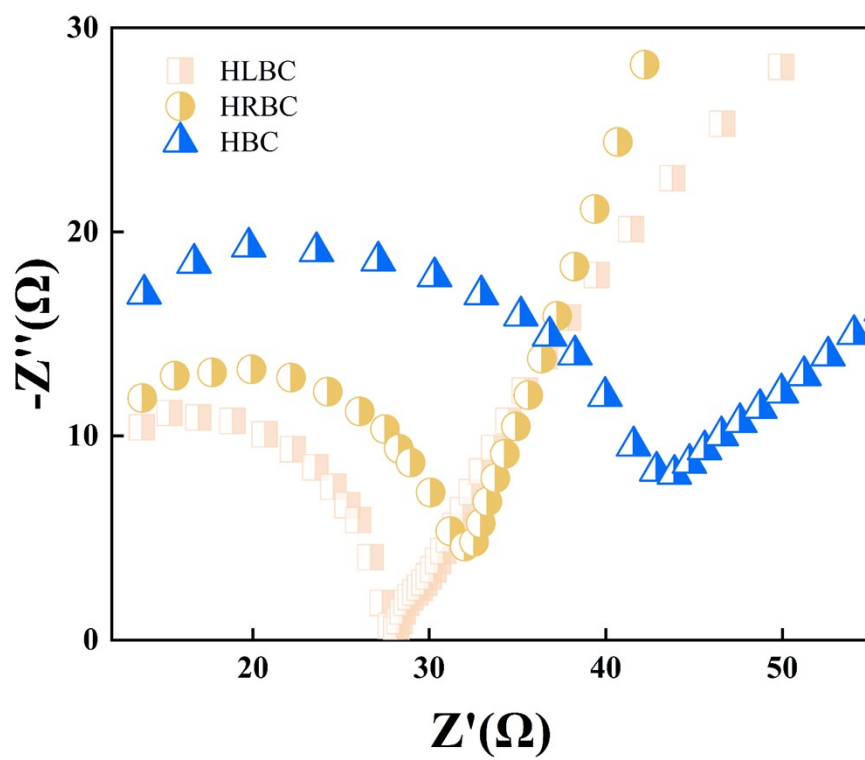


Fig. S21. Electrochemical impedance spectroscopy (EIS) results of HBC, HRBC, and HLBC.

References

- 1 Y. Li, J. Zhang, X. Liu, H. Liu, L. Wang, D. Cheng, Y. Wang, W. Guo and H. H. Ngo, *J. Water Process. Eng.*, 2025, **70**, 107013.
- 2 D. Huang, Q. Zhang, C. Zhang, R. Wang, R. Deng, H. Luo, T. Li, J. Li, S. Chen and C. Liu, *Chem. Eng. J.*, 2020, **391**, 123532.
- 3 W. Xia, B. Song, H. Yi, E. Almatrafi, Y. Yang, Y. Fu, X. Huo, F. Qin, L. Xiang, Y. Zeng, G. Zeng and C. Zhou, *J. Clean. Prod.*, 2022, **373**, 133750.
- 4 S. Ye, G. Zeng, X. Tan, H. Wu, J. Liang, B. Song, N. Tang, P. Zhang, Y. Yang, Q. Chen and X. Li, *Applied Catalysis B: Environmental*, 2020, 269, 118850.